



Molecular basis for the different interactions of congeneric substrates with the polyspecific transporter AcrB

Ivana Malvacio^a, Rosa Buonfiglio^b, Noemi D'Atanasio^b, Giovanni Serra^a, Andrea Bosin^a, Francesco Paolo Di Giorgio^b, Paolo Ruggerone^a, Rosella Ombrato^{b,*}, Attilio Vittorio Vargiu^{a,c,*}

^a Department of Physics, University of Cagliari, s.p. 8, Cittadella Universitaria, 09042 Monserrato, CA, Italy

^b Angelini RR&D (Research, Regulatory & Development), Angelini S.p.A., Piazzale della stazione snc, 00071 S. Palomba-Pomezia, Rome, Italy

^c Bijvoet Center for Biomolecular Research, Faculty of Science - Chemistry, Utrecht University, Padualaan 8, 3584 CH Utrecht, The Netherlands

ARTICLE INFO

Keywords:

AcrB
Efflux pumps
Multidrug resistance
Molecular docking
Molecular dynamics

ABSTRACT

The drug/proton antiporter AcrB, which is part of the major efflux pump AcrABZ-TolC in *Escherichia coli*, is the paradigm transporter of the resistance-nodulation-cell division (RND) superfamily. Despite the impressive ability of AcrB to transport many chemically unrelated compounds, only a few of these ligands have been co-crystallized with the protein. Therefore, the molecular features that distinguish good substrates of the pump from poor ones have remained poorly understood to date. In this work, a thorough in silico protocol was employed to study the interactions of a series of congeneric compounds with AcrB to examine how subtle chemical differences affect the recognition and transport of substrates by this protein. Our analysis allowed us to discriminate among different compounds, mainly in terms of specific interactions with diverse sub-sites within the large distal pocket of AcrB. Our findings could provide valuable information for the design of new antibiotics that can evade the antimicrobial resistance mediated by efflux pump machinery.

1. Introduction

Over-expression of multi-drug efflux pumps of the resistance-nodulation-cell division (RND) protein superfamily is one of the major mechanisms of multi-drug resistance (MDR) in Gram-negative bacteria [1–4]. The paradigm efflux pump of the RND superfamily is the AcrABZ-TolC complex of *Escherichia coli* [5–8], which is composed of the outer membrane protein TolC, the membrane fusion protein AcrA, the small inner membrane protein AcrZ and the RND inner membrane transporter AcrB. The lattermost protein, which is a secondary transporter with a jellyfish-like structure, is fuelled by the transmembrane electrochemical gradient and is responsible for the recognition of a large number of antibiotics (Fig. 1A). The structures of both the symmetric and asymmetric conformations of AcrB, which are thought to represent the resting and active states of the transporter respectively, have been solved by means of X-ray crystallography [9–12]. In the asymmetric structure, each protomer assumes a different conformation corresponding to one of the three states of the proposed functional rotation mechanism: loose (L), tight (T) and open (O) [5,7,13,14]. Transitions among different states involve structural fluctuations in the transmembrane (TM) α -helices due to changes in the protonation states of residues that assist proton flow, as well as the collective movement of

the structural sub-units PN1, PN2, PC1 and PC2 in the periplasmic domain (Fig. 1A) [11,12,15].

Recognition and transport of compounds by this extremely efficient protein seem to occur via multiple pathways, depending on the specific physico-chemical properties of the compounds, although some redundancy is possible [10–12,15–21]. In its simplest form, the functional rotation hypothesis states that recognition of substrates should be initiated at the affinity site known as the access pocket (AP) in monomer L [16,19], which is likely the preferred site for high-molecular-mass (HMM) substrates [19]. After substrate binding, a conformational change from L to T should trigger the movement of substrates towards a deeper site named the distal pocket (DP) [10–12,16], which is believed to be the preferred site for low-molecular-mass (LMM) drugs [19] (Fig. 1B). The AP and DP are separated by a flexible loop (the F617-, switch- or G-loop) [16,19,22], the flexibility of which has been shown to be a pre-requisite for efficient export of some classes of compounds [16,19,23–25]. The DP contains a phenylalanine-rich region known as a hydrophobic trap (HP trap), which contributes to the tight binding of AcrB inhibitors [26–28]. A second conformational change from T to O should trigger substrate release into the central funnel through the exit gate (Gate) [12].

Unfortunately, only a few compounds have been co-crystallized

* Corresponding authors.

E-mail addresses: r.ombrato@angelini.it (R. Ombrato), vargiu@dsf.unica.it (A.V. Vargiu).

<https://doi.org/10.1016/j.bbamem.2019.05.004>

Received 23 February 2018; Received in revised form 20 December 2018; Accepted 6 January 2019

Available online 08 May 2019

0005-2736/© 2019 Elsevier B.V. All rights reserved.

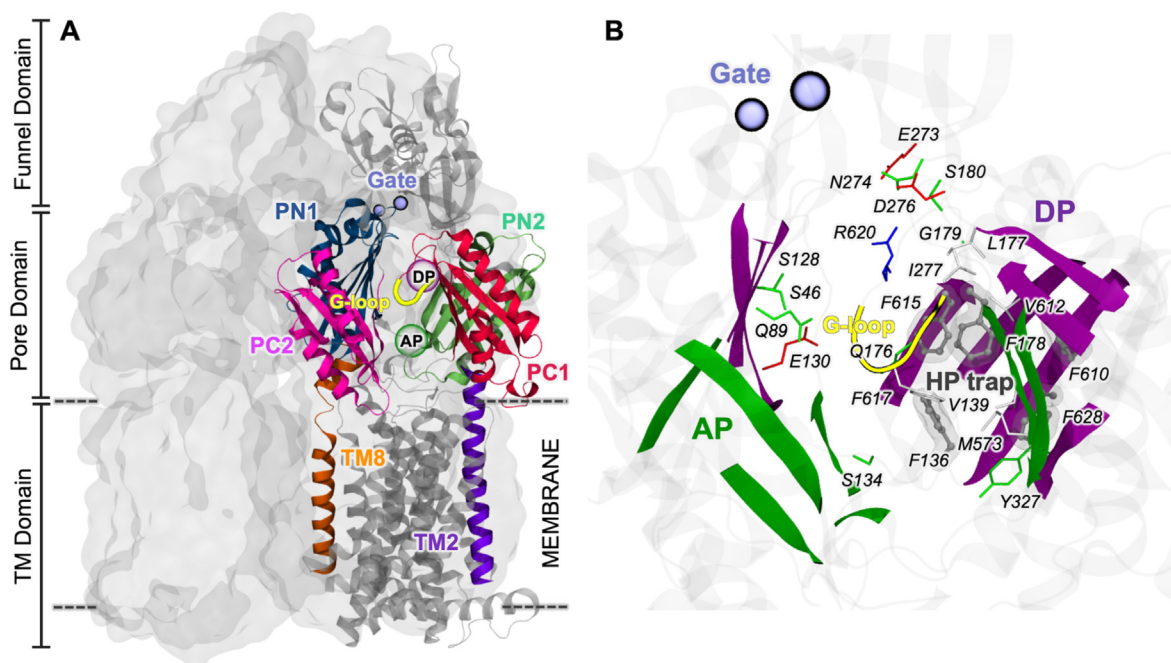


Fig. 1. Structural features of AcrB. (A) The AcrB trimer is shown as a grey transparent surface, whereas monomer T is shown as grey ribbons. Subdomains putatively related to function are shown as coloured ribbons in monomer T (PN1, PN2, PC1, PC2, TM2 and TM8), and key elements such as the exit gate and G-loop are shown as ice-blue spheres and yellow ribbons, respectively. Transparent spheres indicate the approximate positions of the AP (green) and DP (magenta). (B) The AP (green) and DP (magenta) are shown as ribbons, and the exit gate and G-loop are represented in the same manner as in panel A. The residues lining the DP are shown as sticks coloured according to the type of residue, with the exception of the residues lining the HP trap (subsite of the DP) which are shown as grey balls and sticks surrounded by a grey surface.

with AcrB; thus, computational approaches are essential for investigating the determinants of the interactions between diverse ligands and this polyspecific protein. Such knowledge would be crucial for the development of antibiotics (inhibitors) that can evade (inhibit) the efflux machinery. In recent years, a few laboratories, including ours, have performed several studies to examine the mechanism of substrate recognition of different compounds, putative inhibition pathways, effects of mutagenesis, mechanism of action, etc. (see e.g. [29,30] for recent reviews). However, none of these studies addressed the interplay between the physico-chemical properties of a set of different compounds and the susceptibility of these compounds to AcrB.

Prompted by this scenario, we determined how subtle chemical differences within a series of congeneric compounds affect their interactions with AcrB. Namely, we selected seven small molecules (1–7 in Fig. 2) deriving from a hit-finding and optimization campaign carried out to discover novel bacterial topoisomerase inhibitors (NBTIs) with activity against the type IIA topoisomerases (namely, DNA gyrase and topoisomerase IV) and promising antibacterial activity, particularly against Gram-negative strains (G. Magarò et al., submitted). Because DNA gyrase is composed of GyrA₂/GyrB₂ sub-units and topoisomerase IV consists of ParC₂/ParE₂ sub-units, these proteins will be referred to as GyrA and ParC, respectively. Compounds 1–7 showed minimal inhibition concentrations (MICs) ranging from 0.5 to > 16 μM against *E. coli*. Moreover, the compounds exhibited decreased MIC values in *E. coli* strains engineered for deletion of the polyspecific transporter AcrB, suggesting that all the compounds were substrates of this transporter, although to different extents (Table 1). However, since fold changes in MICs often don't correlate with those obtained in experiments that determine efflux activity directly [31], we performed *in silico* atomistic investigations (by means of molecular docking, molecular dynamics - MD - simulations and free energy calculations) in order to rationalize the contribution of specific structural motifs to observed biological data. Because these compounds can be classified as LMM molecules, we focused on the DP within the T monomer of the transporter, which is

the putative recognition site for these kinds of substrates [14,32]. Our work provides meaningful insights of the driving forces to AcrB liability by the different compounds, thus linking their different susceptibilities to deletion of the *acrB* gene to the property of being good or poor substrates of the transporter.

2. Materials and methods

2.1. Chemical compounds

Proprietary compounds were prepared at Angelini as described in the international patent application WO2016096686A1 [33].

2.2. Pharmacology and microbiology

2.2.1. Gel-based enzyme assays

E. coli DNA gyrase supercoiling and topoisomerase IV decatenation assay kits were provided by Inspiralis (Norwich, UK). Assays were performed according to the manufacturer's instructions. Compounds were serially diluted (1:3 dilutions starting from a final concentration of 300 μM) in the reaction mixture and assayed to obtain concentration-response curves in two replicate experiments. The final DMSO concentration in the assays was 1% (v/v). Each reaction was stopped by the addition of 30 μl of chloroform/isoamyl alcohol (26:1) and 30 μl of stop dye (40% sucrose, 100 mM Tris-HCl (pH 7.5), 1 mM EDTA, 0.5 μg/ml bromophenol blue) before loading the samples on a 1.0% TAE (0.04 mM Tris-acetate, 0.002 mM EDTA) gel, which was then run at 80 V for 2 h. Bands were visualized by ethidium staining for 10 min, destained for 10 min in water, analysed by gel documentation equipment (Syngene, Cambridge, UK) and quantitated using Syngene Gene Tools software. Raw gel data (fluorescent band volumes) were converted by the software to a percentage of the control (fully supercoiled or decatenated DNA band).

The data were then analysed using SigmaPlot Version 12.3 (2013).

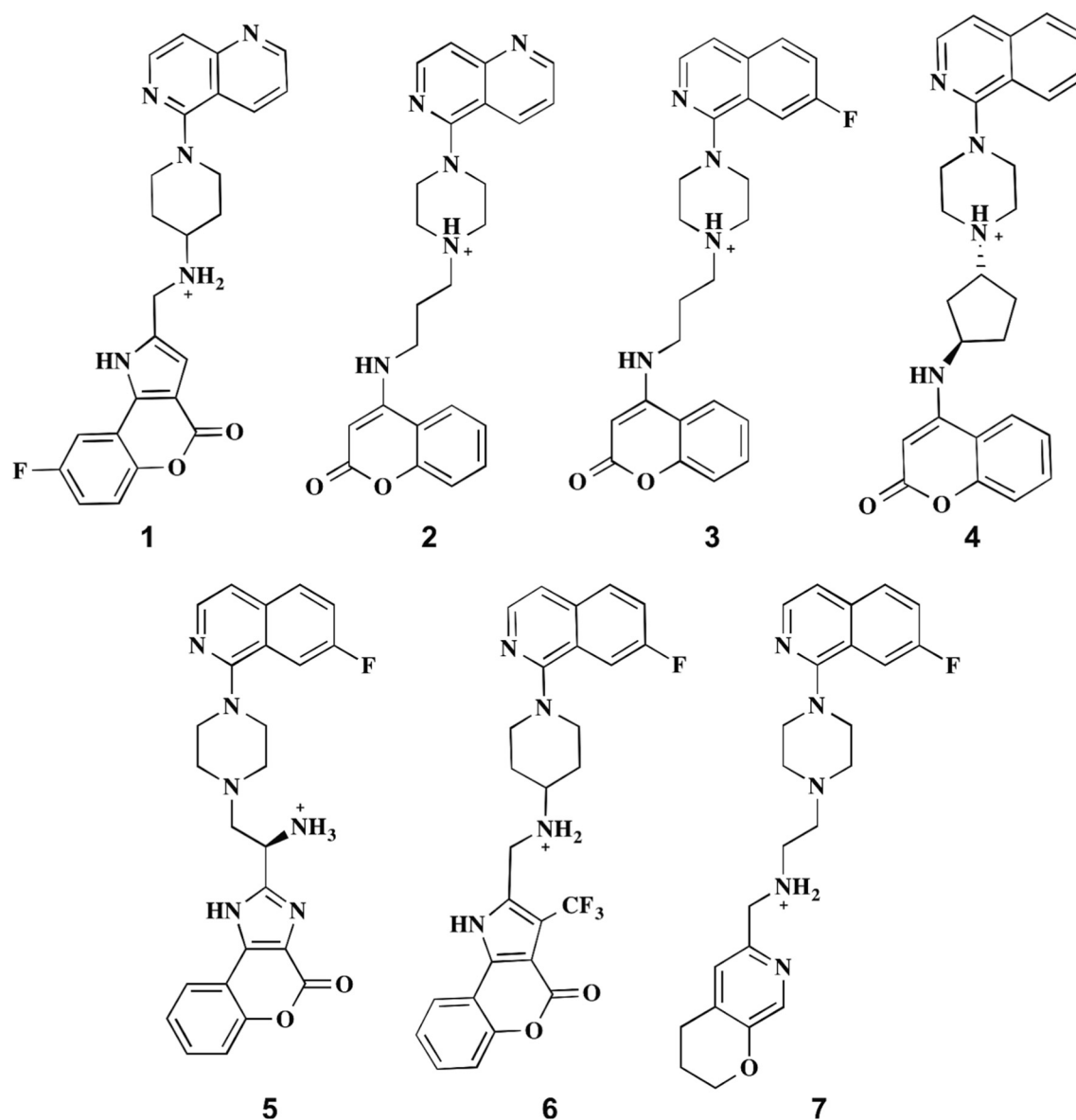


Fig. 2. Library of compounds considered here. Only the predominant structures under physiological pH are shown.

Table 1

Half maximal inhibitory concentrations (IC₅₀ values) of GyrA and ParC of *E. coli* along with the minimal inhibitory concentrations (MICs) of the parent and mutant (Δ acrB) strains.

| Compound | IC ₅₀ [μ M] | | MIC [μ g/mL] | | Fold difference (parent vs. mutant) |
|----------|-----------------------------|------|-------------------|--------------------------------|-------------------------------------|
| | GyrA | ParC | Parent strain | Mutant strain (Δ acrB) | |
| 1 | 0.19 | 1.57 | 0.5 | 0.03 | 4 |
| 2 | 40.6 | 29.3 | 16 | 1 | 4 |
| 3 | 0.80 | 1.7 | 2 | 0.13 | 4 |
| 4 | 19.5 | 6.8 | > 16 | 2 | > 3 |
| 5 | 1.86 | 0.92 | > 16 | 4 | > 2 |
| 6 | 1.42 | 1.34 | > 16 | 4 | > 2 |
| 7 | 17.1 | 4.24 | > 16 | 8 | > 1 |

The global non-linear regression and curve fitting tool was used to calculate the IC₅₀ values. The results were expressed as average values obtained after IC₅₀ calculation for each replicate run.

2.2.2. Bacterial strains

The *acrB* mutant bacterial strain (ORF *E. coli* clone ID: JW0451 # OEC4987-200826007-efflux defective DEL-*acrB*) and its parent strain (Keio knockout parent strain BW25113 (glycerol stock) # OEC5042) were obtained from Dharmacon, GE Healthcare, and stored frozen with 10% glycerine at Eurofins Munich.

2.2.3. Antibacterial susceptibility testing

MICs were determined by broth microdilution according to CLSI guidelines [34,35]. Compounds obtained as DMSO-soluble powders were used for MIC determination following the scheme suggested by the CLSI for preparing dilutions of water-insoluble antibacterial agents [36]. The MIC values of antibiotics used in clinical practice were interpreted according to the susceptibility interpretive criteria reported in the appropriate CLSI tables [36].

2.3. Computational modelling

2.3.1. Molecular docking

To improve the *in silico* prediction of the binding modes of the various compounds at the DP of AcrB, we performed guided ensemble

docking calculations [37–39] for this site using the commercial package Schrödinger's Glide [40]. The goal of this step was to identify robust ligand-AcrB complexes for subsequent computational investigations.

2.3.2. Generation of AcrB conformations

We generated an ensemble of conformations of AcrB featuring the largest structural variance at the DP of monomer T, which is putatively involved in the recognition of the congeneric compounds investigated in this work. Notably, these conformations were either crystallographic structures or conformations extracted from state-of-the-art MD simulations [41,42]. Specifically, we performed cluster analysis on the following structures: i) 15,000 conformations extracted from previous MD simulations of AcrB that were free of ligand and embedded in a model bilayer membrane [32]. These simulations exhibited different geometries of the DP, corresponding to relatively closed pocket conformations compared to published crystallographic structures. ii) 15,000 conformations extracted from a set of MD simulations of AcrB in a 0.15 M solution of benzene, a solvent that is supposed to be expelled by AcrB [43]. The uptake of benzene is associated with an increase in the volume of the DP, improving the conformational diversity at this site compared to that of the partly collapsed geometries sampled along MD trajectories of the ligand-free transporter [32]. The cluster analysis was performed on the cumulative set of structures (30,000 conformations) using the hierarchical agglomerative algorithm implemented in the *cpptraj* module of AMBER 16 [44] and the overall heavy-atom RMSD of the DP of monomer T (see Table S1 for a definition of the residues lining this as well as other key regions of AcrB) as a parameter with a cut-off of 1 Å. Despite this cut-off is relatively low, it was so chosen on purpose because of the known impact of even minor sidechain displacements on docking results. Structures were aligned to the DP prior to evaluation of the RMSD of this site to maximize local structural diversity within the ensemble of cluster representatives. Only the representatives of clusters with populations higher than 1% were retained in the ensemble, resulting in a total of 30 AcrB structures. Finally, 6 crystallographic structures of AcrB (corresponding to PDB IDs 2DHH [10], 2GIF [11], 2J8S [12], 3W9H [26], 4C48 [45] and 4DX5 [16]) were added to the ensemble of conformations derived from MD simulations. These structures were selected from a pool of 21 crystallographic structures (see Table S2) [46] that included both asymmetric (LTO) and bound-to-ligand symmetric (LLL) structures. The structures were aligned to their respective DPs, and the RMSDs were calculated for all possible pairs, resulting in a symmetric 21 × 21 matrix. From this matrix, we retained only the structures that exhibited RMSDs (calculated for all the heavy atoms of the DP) larger than 1 Å from each other. For pairs with RMSDs values below this threshold, we removed the structure with the lowest resolution from the pool, which resulted in the 6 structures mentioned above being included in the ensemble (Table S2). The total number of AcrB conformations used in the ensemble docking runs was thus 36.

2.3.3. Ligand preparation and ensemble docking

The ligands used in this study were converted to 3D structures and prepared with Schrödinger's LigPrep tool [47]. This tool internally calls another Schrödinger package, Epik [48,49], to assign the most probable protonation states and tautomers to each molecule; for the purposes of this work, the software was instructed to consider states that would be dominant at a pH of 7 ± 2 . Chiral centres were enumerated, allowing a maximum of 32 isomers to be produced from each input structure. A conformational search was also carried out using ConfGen (version 3.2) [50]. Overall, the two most likely protonation states were considered for each ligand and all the structures were docked into the AcrB ensemble. However, here, only the predominant species at the physiological pH, corresponding to the protonated structures, were considered for the analysis. These minimized structures constituted the input dataset for the subsequent studies.

Glide required the identification of an approximate binding site on all of the 36AcrB structures, which was achieved by centering each of

them on the centroid defined by carefully selected residues (residue numbers 46, 89, 128, 130, 134, 136, 176, and 620 of the T monomer). The 'docking box', used to inform Glide of the approximate binding site, was then specified as a $20 \times 20 \times 20 \text{ \AA}^3$ box. The ligands were docked into the active site of each AcrB structure and evaluated by the two scoring functions built into Glide: standard precision (SP) and extra precision (XP) [40,51,52]. Since XP performs a more extensive sampling than SP, the structures were first docked and scored using Glide SP and then passed through Glide XP for re-docking and re-scoring. For the ensemble docking calculation, two KNIME workflows [53] were developed. The first workflow was used to generate the grid in the deep pocket for the 36 complexes. The second workflow was designed to run the docking calculations using the 36 grids defined in the previous workflow as receptors. XP docking was performed, and 50 poses were generated for each ligand structure. The top 10 poses obtained per ligand for each receptor grid were selected for the following step.

2.3.4. Clustering of docking poses and re-scoring with the MM/GBSA approach

The ensemble docking campaign performed on the pool of AcrB structures selected above resulted in 360 poses per ligand (10 poses per AcrB structure for each ligand). Considering the whole dataset of 7 ligands, a total of 2520 poses were collected, which were scattered across the whole DP (see Results and Discussion). Therefore, a multi-step cluster analysis was performed to select a relevant but tractable number of different binding modes within the DP to be further characterized via MD simulations. This choice was justified by the consideration that polyspecific proteins such as AcrB are supposed to favour diffuse binding of substrates within their multi-functional binding pockets [14,30,32,54,55]. The hierarchical agglomerative clustering algorithm implemented in the *cpptraj* module of the AMBER16 package [44] was used. The first clustering was carried out using a cut-off of 8 Å for the overall mass-weighted RMSD of the ligand, in order to identify different sub-sites within the large and malleable DP of AcrB (Fig. S1). A second clustering, using a cut-off of 2.0 Å for the overall mass-weighted RMSD of the ligand, was thus performed on each cluster identified in the first step, in order to select a representative structure for each different binding mode. Both the docking score and the population of each cluster were considered to choose the poses to be used as starting structures in MD simulations (vide infra). Notably, we used the *Emodel* score as a metric to rank the poses, as it is customary for selection of the best pose of a ligand (pose selection) when using the Glide package [40]. The average score of the best four poses within each cluster was considered to rank the clusters obtained from the first step, while the score associated to the top pose was used in the second step (Fig. S2). Representative poses of the most populated cluster were selected only if they were associated with a good score (≤ -75). In addition, poses belonging to low populated clusters were added if they were associated with very good scores (≤ -85). Up to 10 top poses were selected (depending on clustering results; we did not set the number of clusters a priori) for each ligand to carry out the subsequent steps. These poses were re-scored by calculating the pseudo-free energy of binding by the Molecular Mechanics/Generalized Born Surface Area (MM/GBSA) approach [56] implemented in AMBER16 [44] (see *Binding Free Energy Calculations* below for further details). The docking score and binding free energy values are reported in Table S3.

2.4. Molecular dynamics simulations

Protomer-specific protonation states were adopted according to [15]: residues E346 and D924 were protonated only in the L and T protomers, while residues D407, D408, and D566 were protonated only in the O protomer, of AcrB. The topology and the initial coordinate files were created using the LEaP module of the AMBER16 package [44]. The proteins were embedded in 1-palmitoyl-2-oleoyl-sn-glycero-3-phosphoethanolamine (POPE) bilayer patches, and the whole

system was solvated with a 0.15 M aqueous KCl solution. The AMBER force field ff14SB [41] was used to represent the protein systems; lipid14 [57] parameters were used for the POPE bilayer; the TIP3P model was employed for water [58], and the parameters for the ions were obtained from [59]. The parameters for the substrates were obtained from the gaff2 force field [42] or generated using the tools of the AMBER16 package when unavailable in the default libraries. In particular, atomic restrained electrostatic potential (RESP) charges were derived using antechamber after structural relaxation of the compounds was performed with Gaussian09 [60] in the density functional theory framework (b3lyp pseudopotential) and using an implicit solvent description.

Each system was first subjected to a multi-step structural relaxation via a combination of steepest descent and conjugate gradient methods using the *pmemd* program implemented in AMBER16, as described in previous publications [22,27,28,32]. The systems were then heated from 0 to 310 K in two subsequent MD simulations: i) from 0 to 100 K in 1 ns under constant-volume conditions and with harmonic restraints ($k = 1 \text{ kcal}\cdot\text{mol}^{-1}\cdot\text{\AA}^{-2}$) on the heavy atoms of both the protein and the lipids; ii) from 100 to 310 K in 5 ns under constant pressure (set to a value of 1 atm) and with restraints on the heavy atoms of the protein and on the z coordinates of the phosphorous atoms of the lipids to allow membrane rearrangement during heating. As a final equilibration step, a series of 20 equilibration runs of 500 ps (total 10 ns), with restraints on the protein coordinates, were performed to equilibrate the box dimensions. These equilibration steps were carried out under isotropic pressure scaling using the Berendsen barostat, whereas a Langevin thermostat (collision frequency of 1 ps^{-1}) was used to maintain a constant temperature. Finally, production MD simulations that were 500 ns in duration were performed for each system. In addition to these simulations of the complexes formed between AcrB and the congeneric compounds, the latter were also simulated for $1 \mu\text{s}$ each in explicit solvent, following the protocol reported in [61].

A time step of 2 fs was used during these runs, while the production phase of the MD simulations was carried out with a time step of 4 fs under an isothermal-isobaric ensemble after hydrogen mass repartitioning [62]. During the MD simulations, the lengths of all the R–H bonds were constrained with the SHAKE algorithm. Coordinates were saved every 100 ps. The Particle mesh Ewald (PME) algorithm was used to evaluate long-range electrostatic forces with a non-bonded cut-off of 9 Å.

2.5. Post-processing of MD trajectories

MD trajectories were analysed using either in-house *tcl* and *bash* scripts or the *cpptraj* tool of the AMBER16 package [44]. Figures were prepared using gnuplot 5.0 [63] and VMD 1.9.2 [64].

2.5.1. Cluster analysis of MD trajectories

Clustering of the ligand trajectories was carried out using the average-linkage hierarchical agglomerative clustering method implemented in *cpptraj* and employing a mass-weighted RMSD cut-off of 3 Å on all the heavy atoms of the ligand. All of the analyses described below but the free energy calculations were performed on all the conformations belonging to the larger cluster populating the second half of the production trajectory, which in most cases coincides with the most populated one (see Figs. S3 and S4).

2.5.2. Solvation free energy calculations

The MM/GBSA approach [56] implemented in AMBER16 [44] was used to calculate the solvation free energy contributions to the binding free energy following the same protocol used in previous studies [22,27,28,65,66]. This approach provides an intrinsically simple method for decomposing the free energy of binding into contributions from single atoms and residues [67]. The solute conformational entropy contribution (TAS_{conf}) was not evaluated [56]. Calculations were

performed on 50 different conformations of each complex, which were extracted from the larger cluster populating the second half of the production trajectory (see Figs. S3 and S4).

2.5.3. Ligand flexibilities

The root mean square fluctuations (RMSFs) of the ligands were calculated using *cpptraj* after structural alignment of each trajectory onto the common molecular scaffold (atom numbers 1–22); see Fig. S5 for a comparison of the flexibilities of the most chemically dissimilar portions of the molecules. This protocol was used to obtain RMSF values from MD simulations of the substrates in complex with AcrB and into explicit water solvent. Temperature B-factors were calculated from the RMSF values using the following formula:

$$B = \frac{8}{3} \pi^2 (\text{RMSF})^2$$

2.5.4. Hydration properties

The average number of water molecules surrounding each substrate in complex with AcrB and in explicit water was estimated with *cpptraj*. For the first (second) hydration layer, we used a distance cut-off of 3.4 (5) Å between the heavy atoms of the ligands and the water oxygens.

2.5.5. Ligand-protein interactions

Analysis of the contacts between each ligand and the hydrophobic, polar and charged residues of AcrB was performed using an in-house *tcl* script run using VMD1.9.2 software. A contact was counted whenever the distance between any atom of the ligand and any atom of each residue was $< 2.5 \text{ \AA}$. Hydrogen bond (H-bond) contacts between the substrate and the transporter were calculated using cut-off values of 3.5 Å for the acceptor-donor distance and of 35° for the donor-hydrogen-acceptor angle.

2.5.6. Structural rearrangements in AcrB

To understand if and to what extent the binding of different substrates induced structural changes in AcrB [68,69], we first evaluated the RMSD values of the transmembrane region (namely, helices TM2 and TM8) and of the joint PC1-PC2 and PC1-PN2 domains of the protein. We used a *tcl* script and calculated structural distortions from both the T and O protomers of the crystallographic structure with PDB ID 4DX5 (which has the highest resolution reported to date) [16]. Prior to the calculation, each domain was aligned to the corresponding domain in the reference structure.

3. Results and discussion

3.1. Biochemical assays

The seven compounds used in this study showed potent dual targeting activity, exhibiting strong inhibition of both the GyrA and ParC enzymes derived from *E. coli* (Table 1). The IC_{50} values were in the range 0.19–40.6 μM for DNA gyrase and 0.92–29.3 μM for topoisomerase IV. The antibacterial activity of these compounds was determined against a wild-type *E. coli* strain and a ΔacrB mutant strain engineered for deletion of the efflux pump protein complex [70–72]. As shown in Table 1, the susceptibility of the *E. coli* *acrB* mutant strain to the different test compounds was higher than that of the parent strain. This finding suggests that the potency of the test compounds is limited by the efflux systems in these bacteria.

3.2. Computational modelling

3.2.1. Molecular docking

To consider all the possible binding modes of each compound within the wide and flexible DP of the polyspecific AcrB transporter [22], an extensive ensemble docking campaign was performed. For each ligand

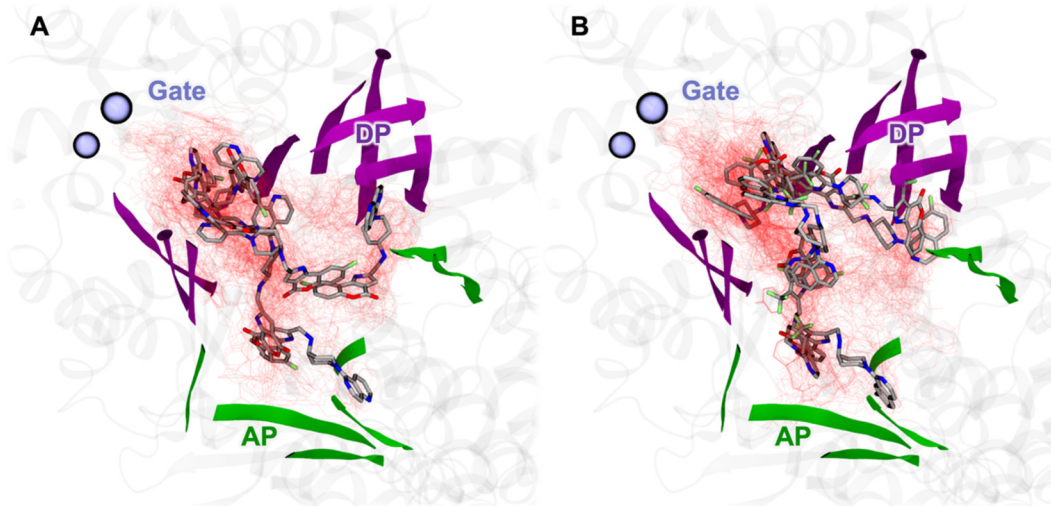


Fig. 3. Distribution of all docking poses (red lines) for compounds **1** (A) and **6** (B). Poses selected for refinement via all-atom MD simulations are shown as sticks coloured by atom name. The structural elements lining the DP and AP are depicted as magenta and green ribbons, respectively, while ice-blue spheres indicate the residues lining the Gate.

shown in Fig. 2, different conformers were generated, and 36 different conformations of AcrB (obtained from crystal structures and previous MD simulations, see *Materials and Methods* for details) were used in docking runs. Overall, we obtained 360 poses for each ligand structure. Visual inspection of the docking results (see Fig. 3 for compounds **1** and **6** as examples) revealed that, for each ligand, the poses were localized throughout the DP. This finding is consistent with the well-known ability of AcrB to recognize several different functional groups at multifunctional sites within the DP (and to allow multiple binding modes of the same ligand), favouring diffuse binding of substrates [14,22,30,32,54,73].

Consistent with the visual data, analysis of the pseudo-affinity values estimated by Glide or via the MM/GBSA approach [56] (Table S3) did not reveal the existence of a strongly preferred binding mode for any of the substrates. Moreover, no clear correlation was observed between any of these pseudo-affinity values and the values of the fold changes on MIC (parent vs. mutant strains) obtained from the susceptibility assay (Table S3). Clearly, selection of only a few poses on the basis of the docking score might be unsuitable for AcrB, not only because of the well-known limitations of the scoring functions [74,75] but also because of the polyspecificity of this transporter [14,76]. Therefore, we hypothesized that a cluster analysis that could capture the distribution of the docking poses would be the most appropriate method for pose selection. Based on the above discussion, a two-step cluster analysis was carried out (see *Materials and Methods* and Figs. S1 and S2 for more details) by using the cumulative ensemble of all the poses for each ligand with all the protein structures. Overall, a reasonable number of different binding modes (up to 10 complex structures) were selected for each compound on the basis of both the cluster population and docking score (see Fig. 3 and Table S3).

3.3. MD simulations and free energy calculations

MD simulations and post-processing analyses were performed systematically for all the complexes selected in the previous step and reported in Table S3. Since hydration of hydrophobic cavities in proteins can be problematic and affect the structure and the dynamics of the complex, for one ligand (compound **6**) we compared the solvation protocol implemented in LEaP with that available in the program solvate_1.0 (<https://www.mpibpc.mpg.de/grubmueller/solvate>). Namely, we compared the number of waters within the first solvation shells of the ligand along the first 50 ns of the MD trajectories. As expected,

despite the relatively large difference in the initial number of waters placed around the ligand (thus also at the hydrophobic trap) by LEaP and solvate_1.0, after a few tens of ns this number converged towards a similar and constant value irrespectively of the methodology used to solvate the system (Fig. S6). Therefore, we are confident that the relatively long equilibration protocol used in our MD simulations guarantees proper hydration of the binding site, including the hydrophobic trap region.

For the sake of clarity, we compare here the binding features of compounds **1** and **6** as representatives of good and poor substrates of AcrB, respectively. This choice allowed us to clearly demonstrate how our protocol is able to elucidate the biological profiles of the two compounds on the basis of their different interactions with AcrB (Table 1). Eight all-atom MD simulations of 0.5 μ s in length were performed for each compound.

(see *Materials and Methods*). While the dynamics did not indicate a common binding mode for any compound, we noticed large displacements of the ligand **1** in two trajectories (Fig. 4A). In particular, the docking poses where the ligand was largely embedded in the HP trap (which is supposedly the preferred binding site for inhibitors [7,26,27,66,77]) were among the most unstable ones and resulted in significant displacement of the compound from the trap, with which only a marginal interaction was maintained (simulations **1.c** and **1.g** in Fig. 4A; see also Figs. S3 and S7). The opposite behaviour was observed for compound **6**, which did not move away from the HP trap in the two docking poses, indicating significant interaction of the ligand with this site (simulations **6.a** and **6.c** in Fig. 4B; see also Figs. S4 and S8). This trend was confirmed by the analyses of the distances between the centres of mass of the ligands and of the HP trap along the MD simulations **1.c**, **1.g**, **6.a** and **6.c** (Fig. S9).

A significantly different behaviour was observed when comparing the binding affinities of the two compounds (namely, the differences in solvation free energies estimated through the MM/GBSA method, which is a computationally cheap alternative to more demanding methods, though it does not include conformational entropy). The binding modes of compound **1** had fairly comparable affinities (ranging from -21.7 to -29.4 kcal/mol, see Table S4) and were distributed from the bottom to the top of the DP and throughout the upper region of the AP but did not involve tight binding to the HP trap, from which the substrate tends to partly escape during MD simulations (Fig. 5A and Table S4). In contrast, compound **6** exhibited a high degree of variation in its calculated binding affinities (from -23.3 to -36.7 kcal/mol).

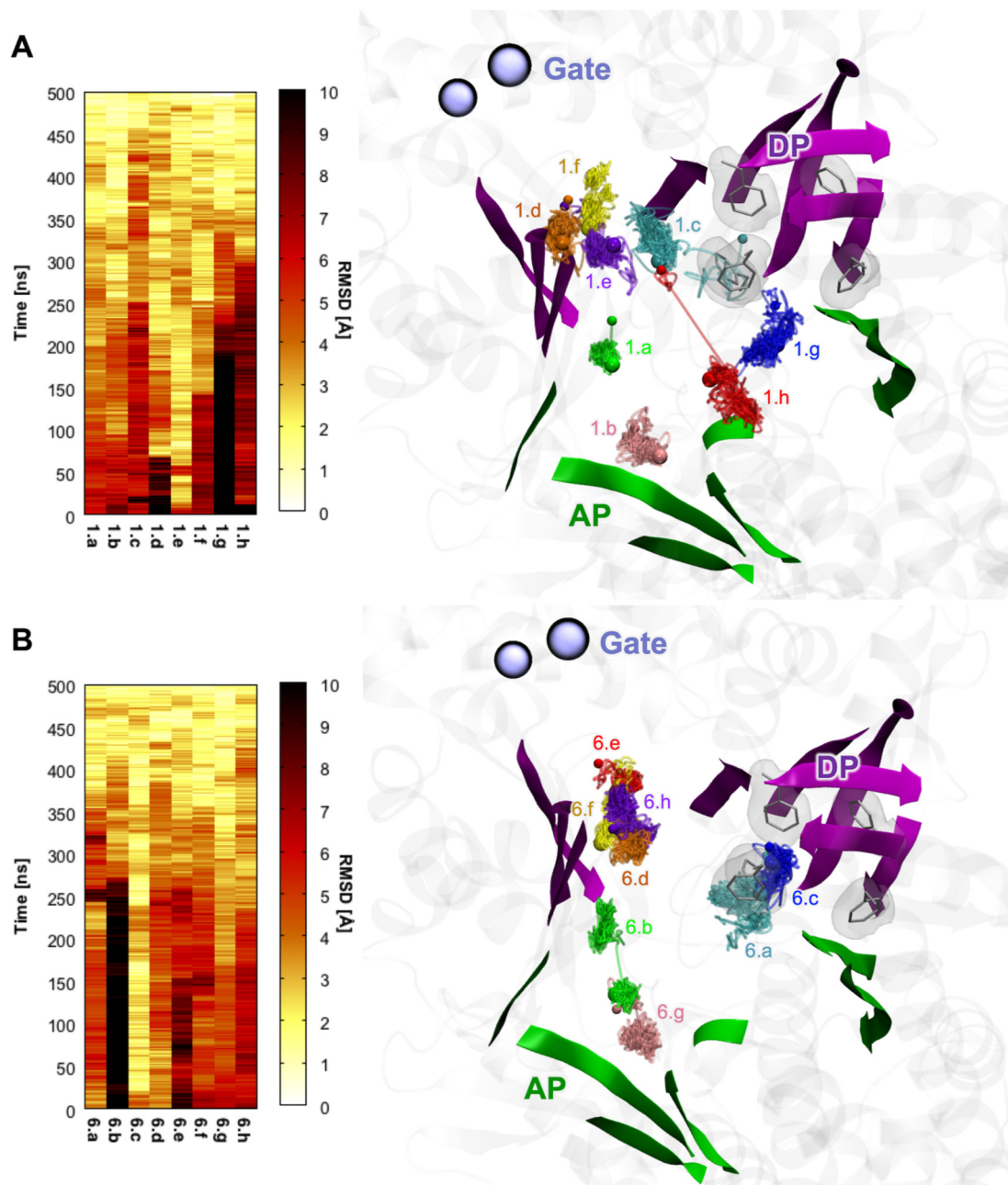


Fig. 4. Ligand RMSDs (with respect to the last frame) along with trajectories of the centres of mass of the ligands during 0.5 μ s MD simulations for (A) 1.a-h and (B) 6.a-h. Small spheres represent the centres of mass of the docking poses, while the large spheres represent the final pose.

Moreover, the binding modes within the AP (6.g) and the HP trap (6.c) exhibited the highest affinities (Fig. 5B and Table S4).

These results are consistent with and provide a rationale for the findings reported in Table 1, which indirectly suggest that 1 is a better AcrB substrate than 6. Indeed, according to the diffuse binding hypothesis recently proposed to explain polyspecificity in AcrB [14,54], an ensemble of binding modes with similarly low affinities within the DP should be compatible with efficient export. On the other hand, the high affinity of 6 for the AP and particularly for the HP trap, which is known to be a preferred interaction site for inhibitors [22,26–28,77], should result in an increased dwelling time of this compound within the protein, thus impairing transport, as observed for some inhibitors or substrates in mutants with defective AcrB proteins [7,29,78].

In addition to the (solvation) binding free energy, to select the most likely binding modes for further analysis we also considered the structural stability of the poses during the MD simulations. Below, we

describe in detail only the highest affinity binding modes that featured a stable position and orientation of the ligand. For compound 1, the two binding modes with highest affinity were located at the top (1.e, with affinity -27.7 kcal/mol) and bottom of the DP (1.g, with affinity -29.4 kcal/mol), but only the former was stable during the entire second half of the MD trajectory (Fig. 4A). On the other hand, the highest affinity binding modes of 6, located in the upper region of the AP (6.g, with affinity -36.7 kcal/mol) and within the HP trap (6.c, with affinity -31.8 kcal/mol), were both stable (Fig. 4B).

Here, we compare the features of complexes 1.e and 6.c, 6.g, focusing on 1) the differences in the structural and physico-chemical properties of the complexes, 2) the details of the interactions of the ligands with AcrB, and 3) the key conformational changes induced by the ligands in AcrB. We first analysed the changes in ligand flexibility upon binding, evaluated as the differences in the RMSF values of the ligand in complex with AcrB with respect to the values calculated in

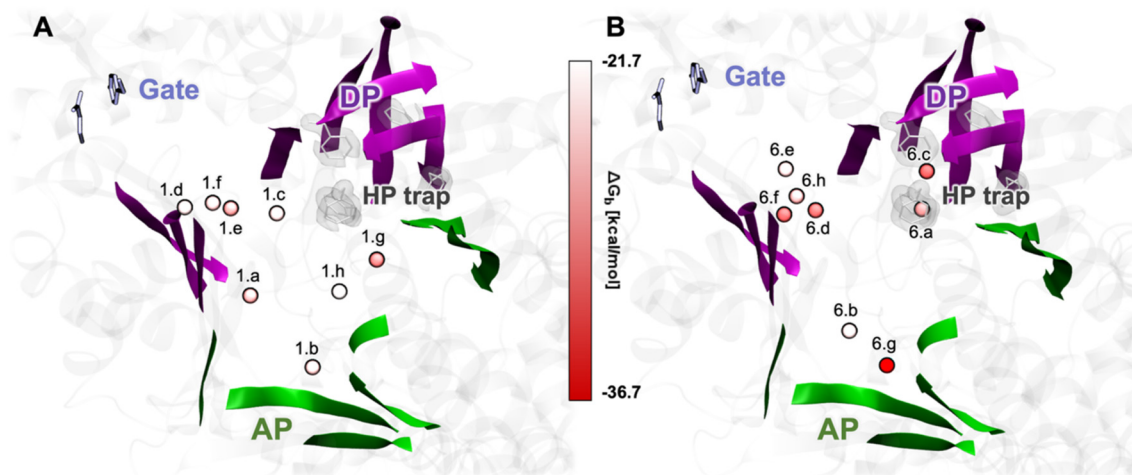


Fig. 5. Distribution and binding affinities of the poses of (A) **1** and (B) **6** within the DP and the AP of AcrB. The spheres represent the centre of mass of the ligand structure closest to the average during the stable part of the trajectory and are coloured by ΔG_b value according to the colorimetric scale shown in the middle of the figure. The DP and AP are depicted as cartoon representations in magenta and green, respectively. The Phe residues of the HP trap are shown as grey surfaces, and the residues lining the exit gate are shown as ice-blue sticks.

Table 2
Ligand dehydration upon binding to AcrB.

| Ligand Binding mode | Average number of water molecules | | | | Number of lost water molecules | |
|---------------------|-----------------------------------|-----------|-------------|-----------|--------------------------------|-----------|
| | Ligand-water | | Ligand-AcrB | | | |
| | 1st shell | 2nd shell | 1st shell | 2nd shell | 1st shell | 2nd shell |
| 1.e | 20 ± 3 | 75 ± 4 | 5 ± 1 | 12 ± 3 | 15 | 63 |
| 6.c | 22 ± 3 | 79 ± 4 | 4 ± 1 | 8 ± 2 | 18 | 71 |
| 6.g | | | 3 ± 1 | 6 ± 2 | 19 | 73 |

water (see Materials and Methods). Very similar Δ RMSF profiles were obtained (Figs. S5A–C), indicating similar flexibilities of the two molecules, with only a slight difference observed between the naphthyridine and fluoroisoquinoline groups. In addition, we estimated the extent of ligand dehydration by calculating the relative loss of water molecules from the first and second solvation shells of the substrates (Table 2). A slightly greater desolvation was observed for **6.c** and **6.g**, an effect related to the higher lipophilicity of this ligand (compared to **1**) imparted by the greater number of fluorine atoms in its structure, leading to the prevalence of hydrophobic contacts made by this ligand. According to the recently proposed water-mediated transport mechanism for AcrB, substrate transport from the DP to the funnel domain of AcrB should occur within a channel, allowing fairly constant hydration of compounds [79]. Therefore, the higher hydration of **1** (Table 2) than that of **6** within AcrB should facilitate smoother diffusion of the former compound through the protein channels.

Next, we analysed the structure, dynamics and energetics of the interactions between the two compounds and AcrB in detail. Fig. 6 (bottom panel) summarizes the percentages of contacts of each compound with different residue types, as well as those mediated by water. A balanced distribution of contacts with hydrophobic, polar and charged residues in addition to H-bonds and water-mediated interactions (Fig. 6A) was observed for **1.e**, which is consistent with the smooth interactions established by this compound with many different sub-sites within the DP. Notably, similar results were obtained from the analysis of per-residue contributions to ΔG_b (Table S5). Thus, in addition to the relatively low and similar affinities of **1** to different subsites within the DP of AcrB, in its preferred binding mode, this compound is unable to form strong interactions of one particular type. This feature is desirable for a substrate because strong specific interactions could hinder the diffusion of the substrate away from the recognition site

[79]. In contrast, a clear prevalence of contacts with hydrophobic residues was observed for both **6.c** in the HP trap and **6.g** within the AP (Fig. 6B–C). In addition, hydrophobic residues are the greatest contributors to binding affinity, as shown in Table S5.

Binding affinity is frequently found to be associated with hydrophobic interactions and can be optimized by incorporating this kind of interactions in place of H-bonds [80]; thus, the fluorine substituents present in **6** led to slight enhancement of the binding affinity (Table S4) due to increased lipophilicity [80–82]. Notably, a similar percentage of H-bonds and water-bridged interactions were observed for **1.e** and **6.g**, while in **6.c**, the number was considerably reduced. This decrease was also expected due to the large fraction of hydrophobic residues lining the HP trap [26]. Fig. 6 (top panel) shows representative conformations of complexes **1.e**, **6.g** and **6.c**, highlighting the main interactions formed between the ligands and AcrB in the highest affinity binding modes. In **1.e**, the compound established two long-lived H-bonds: one between N6 of naphthyridine and the guanidinium group of the R620 side chain (present for 62% of the total simulation time) and another between the ammonium group of the ligand and the side-chain carboxyl group of E130 (present for 76% of the time). In addition, several water-bridged interactions were formed (in Fig. 6A, we show two of these interactions, involving Q125 and L177). In **6.g**, the ligand established a highly conserved H-bond (present for 91% of the time) with the side-chain carboxyl group of E673 via its pyrrole NH and ammonium groups, which was strengthened by a water-bridged H-bond formed by the N atom of isoquinoline (Fig. 6B). Finally, hydrophobic contacts with residues F136, F178 and F628 were prevalent in the binding of **6.c** within the HP trap (Fig. 6C).

The conformational changes induced on AcrB in **1.e**, **6.c** and **6.g** were evaluated by monitoring the RMSDs of important domains along the MD trajectory. In particular, because it is accepted that the binding of substrates activates transport by triggering conformational changes in AcrB [6], we evaluated the evolution of the RMSD of selected domains (TM helices 2 and 8 and joint domains PC1-PC2 and PC1-PN2) with respect to the T and O conformations found in the highest resolution crystallographic structure of the transporter [16]. No significant differences were observed in the structural changes induced on the protein by the two ligands, with the exception of the changes induced on the TM8 helix. Indeed, this helix underwent an appreciable conformational change in **1.e**, for which similar RMSD values were obtained from both the T and O conformations (Fig. 7 and Table 3), whereas the helix remained much closer to the T state in both **6.c** and **6.g**. The structure assumed by TM8 in **1.e** could represent a transient

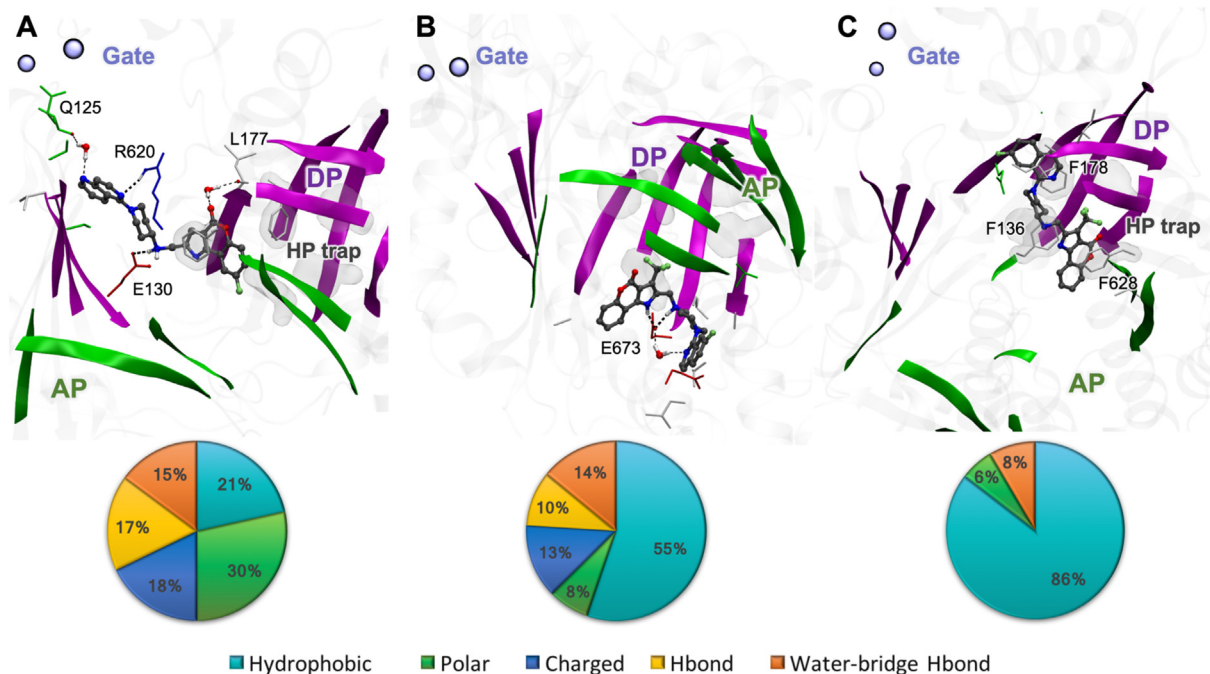


Fig. 6. Representative binding modes (top) and percentages of contacts (bottom) of A) 1.e in the upper region of the DP, B) 6.g in the AP and C) 6.c in the HP trap. Residues within 2.5 Å of the ligand are shown as thick and are coloured by residue type (polar: green, hydrophobic: white, negatively charged: red, and positively charged: blue). The DP and AP are exhibited as magenta and green ribbons, respectively, while the residues lining the gate are shown as ice-blue spheres. The percentages of contacts with hydrophobic, polar and charged residues are shown in cyan, green and blue, respectively; H-bonds are shown in yellow, and water-bridge interactions are shown in orange.

conformation between the two crystallographic states associated with binding to and unbinding from the DP [7,15].

Because the initial structures of AcrB in the highest affinity binding modes 1.e and 6.g were different, we decided to validate our findings by also comparing the behaviour of TM8 in simulations starting from the same AcrB structure. Two examples of such complexes are 1.g and

6.c, in which the crystallographic structure 4DX5 [16] was used as the receptor. Even though both binding modes featured the compounds within the HP trap, only 1.g induced a significant conformational change in TM8, leading this helix to assume an intermediate conformation between the T and O states (RMSD_T from 0.4 to 2.7 Å and RMSD_O from 4.5 to 3.5 Å), whereas in 6.c, the ligand induced only a

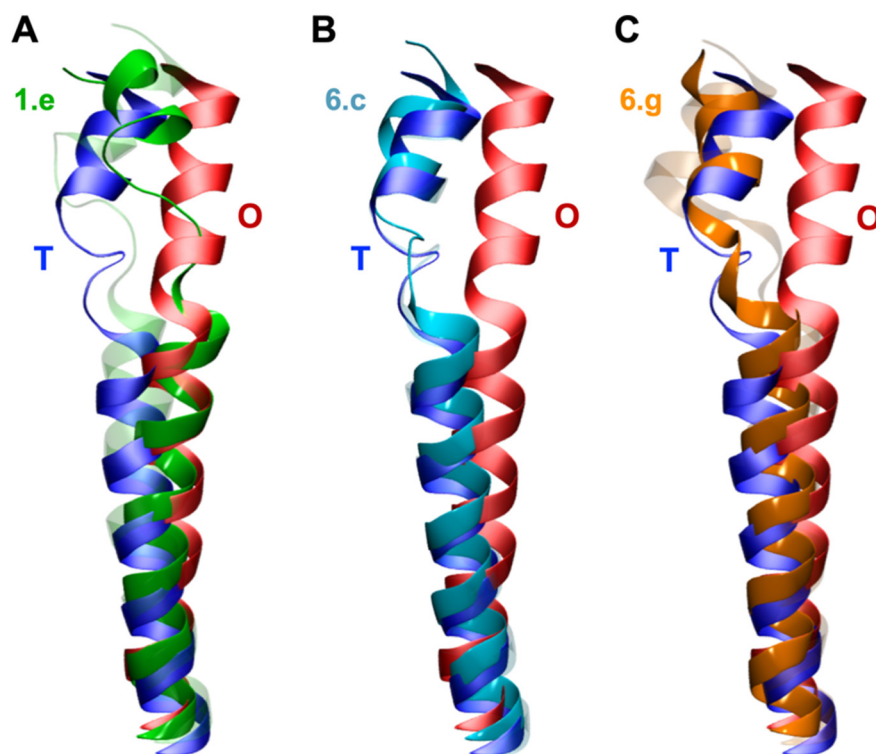


Fig. 7. Conformational changes induced in TM8 (after alignment of the whole transmembrane region of AcrB) by the binding of different substrates to AcrB. The structures of the helix in the T and O states are exhibited as blue and red ribbons, respectively, whereas the initial (transparent) and final (solid) conformations in 1.e (A), 6.c (B), and 6.g (C) are shown as green, cyan and orange ribbons, respectively.

Table 3

RMSD values of TM8 with respect to the T and O conformations of AcrB in the crystallographic structure PDB ID 4DX5 [16] (after structural alignment of the whole transmembrane AcrB region). Initial values refer to the first frame of the equilibration phase (immediately after structural relaxation), and average RMSDs (with standard deviations in parentheses) were obtained from the last 100 ns of the production MD.

| Complex | Initial value | | Average (last 100 ns) | |
|------------|-----------------------|-----------------------|-----------------------|-----------------------|
| | RMSD _T [Å] | RMSD _O [Å] | RMSD _T [Å] | RMSD _O [Å] |
| 1.e | 3.0 | 4.8 | 3.5 (0.2) | 3.8 (0.3) |
| 6.c | 0.4 | 4.5 | 1.7 (0.2) | 4.9 (0.2) |
| 6.g | 2.8 | 5.1 | 2.8 (0.2) | 4.8 (0.3) |

small rearrangement (RMSD_T from 0.4 to 1.7 Å and RMSD_O from 4.5 to 4.9 Å), confirming previous findings. Clearly, due to the relatively short timescale affordable with all-atom MD simulations of these systems (up to a few μs [30]) compared with the timescale associated with efflux by AcrAB-TolC (a few ms, see e.g. [6,66,77]), we expected to see no further structural movement, such as those observed for the entire functional cycle.

4. Concluding remarks

In this work, we studied the interaction of a series of congeneric compounds with the major RND transporter AcrB of *E. coli*. Microbiological and pharmacological experiments showed that despite the large degree of chemical and structural similarity among the seven compounds considered in this work, the interactions of these molecules with AcrB differed significantly. As AcrB is the paradigm RND-type multi-drug efflux transporter in Gram-negative bacteria, elucidation of the subtle differences in the physico-chemical parameters of compounds that determine their suitability as protein substrates has crucial implications for both basic research and drug design. While a generic requirement for a certain degree of lipophilicity has been proposed since the discovery of AcrB [6], the link between the structural and chemical fingerprints of compounds and the peculiar physico-chemical properties of the multi-drug binding sites in this and homologous proteins has been investigated quantitatively only in recent years [32,83].

With the aim of rationalizing the experimental findings at the molecular level, we used a multi-disciplinary computational protocol that allowed us to identify a series of specific molecular determinants that are crucial for the interactions between compounds and AcrB. We focused our computational efforts on two molecules, named **1** and **6**, which are representative of a good and poor substrate of AcrB, respectively. An ensemble of binding modes with similar and relatively low affinities was identified for compound **1** within the DP, which should be compatible with efficient export based on the diffuse binding hypothesis proposed a few years ago to rationalize the polyspecificity of AcrB [14]. Indeed, a balanced distribution among different interaction types was observed between AcrB and this compound, which is consistent with the smooth interactions it established with many different sub-sites within the DP. On the other hand, the high affinity of **6** for the AP and particularly for the HP trap (due to the slightly higher lipophilicity of this compound, resulting in the prevalence of hydrophobic interactions within the binding pocket), should result in an increased dwelling time of this compound within the protein, thus, impairing transport as observed with some inhibitors or substrates in mutants with defective AcrB [7,78]. In addition, the greater hydration of **1** compared to **6** within AcrB should facilitate smoother diffusion of the former compound through protein channels [79]. Finally, **1** induced conformational changes in TM8 [15] of AcrB, leading to a state partly in T and partly in O, whereas this transporter remained much closer to the T state in the presence of **6**. Such conformational changes have been hypothesized to be part of the concerted movements that trigger the

functional rotation of AcrB.

Clearly, in view of the partial overlap among the pool of AcrB substrates and those of other transporters such as AcrD and AcrF [6,7], we cannot rule out a role for these additional proteins in altering the susceptibilities of *E. coli* to the congeneric compounds investigated here. Nonetheless, we believe that this work contributes to the understanding of how the subtle balance among different physico-chemical features reflect on their interaction with AcrB and identifies the parameters that can be tuned to regulate the strengths of such interactions.

Transparency document

The Transparency document associated with this article can be found in online version.

Acknowledgements

We thank Dr. Giuliano Mallocci (University of Cagliari) for useful discussions regarding the docking protocol used in this work. The research presented in this work has been funded by Angelini through the project “Structural and thermodynamical characterization of multiple-site binding of substrates to the RND transporter AcrB of *E. coli*” (to A. V. Vargiu).

Declaration of Competing Interest

R. Buonfiglio, N. D'Atanasio, F. P. Di Giorgio, and R. Ombrato are employees of Angelini, which funded this research under the project “Structural and thermodynamical characterization of multiple-site binding of substrates to the RND transporter AcrB of *E. coli*”. Ivana Malvacio is a recipient of a post-doctoral fellowship under the same project.

Appendix A. Supplementary data

Supplementary data to this article can be found online at <https://doi.org/10.1016/j.dummy.2019.01.002>.

References

- [1] E.D. Brown, G.D. Wright, antibacterial drug discovery in the resistance era, *Nature* 529 (2016) 336–343.
- [2] H. Inoue, R. Minghui, Antimicrobial resistance: translating political commitment into national action, *Bull. World Health Organ.* 95 (2017) 242.
- [3] D.J. Payne, Microbiology desperately seeking new antibiotics, *Science* 321 (2008) 1644–1645.
- [4] D.J. Payne, M.N. Gwynn, D.J. Holmes, D.L. Pompliano, Drugs for bad bugs: confronting the challenges of antibacterial discovery, *Nat. Rev. Drug Discov.* 6 (2007) 29–40.
- [5] D. Du, H.W. van Veen, B.F. Luisi, Assembly and operation of bacterial tripartite multidrug efflux pumps, *Trends Microbiol.* 23 (2015) 311–319.
- [6] X.-Z. Li, P. Plésiat, H. Nikaido, The challenge of efflux-mediated antibiotic resistance in gram-negative bacteria, *Clin. Microbiol. Rev.* 28 (2015) 337–418.
- [7] P. Ruggerone, S. Murakami, K.M. Pos, A.V. Vargiu, RND efflux pumps: structural information translated into function and inhibition mechanisms, *Curr. Top. Med. Chem.* 13 (2013) 3097–3100.
- [8] H.I. Zgurskaya, J.W. Weeks, A.T. Ntrel, L.M. Nickels, D. Wolloscheck, Mechanism of coupling drug transport reactions located in two different membranes, *Front. Microbiol.* 6 (2015).
- [9] S. Murakami, R. Nakashima, E. Yamashita, A. Yamaguchi, Crystal structure of bacterial multidrug efflux transporter AcrB, *Nature* 419 (2002) 587–593.
- [10] S. Murakami, R. Nakashima, E. Yamashita, T. Matsumoto, A. Yamaguchi, Crystal structures of a multidrug transporter reveal a functionally rotating mechanism, *Nature* 443 (2006) 173–179.
- [11] M.A. Seeger, A. Schiefner, T. Eicher, F. Verrey, K. Diederichs, K.M. Pos, Structural asymmetry of AcrB trimer suggests a peristaltic pump mechanism, *Science* 313 (2006) 1295–1298.
- [12] G. Sennhauser, P. Amstutz, C. Briand, O. Storchenegger, M.G. Grütter, Drug export pathway of multidrug exporter AcrB revealed by DARPIn inhibitors, *PLoS Biol.* 5 (2007).
- [13] K.M. Pos, Drug transport mechanism of the AcrB efflux pump, *Biochim. Biophys. Acta BBA Proteins Proteomics* 1794 (2009) 782–793.
- [14] A. Yamaguchi, R. Nakashima, K. Sakurai, Structural basis of RND-type multidrug

- exporters, *Front. Microbiol.* 6 (2015).
- [15] T. Eicher, M.A. Seeger, C. Anselmi, W. Zhou, L. Brandstätter, F. Verrey, K. Diederichs, J.D. Faraldo-Gómez, K.M. Pos, Coupling of remote alternating-access transport mechanisms for protons and substrates in the multidrug efflux pump AcrB, *Life* 3 (2014) e03145.
- [16] T. Eicher, H. Cha, M.A. Seeger, L. Brandstätter, J. El-Delik, J.A. Bohnert, W.V. Kern, F. Verrey, M.G. Grütter, K. Diederichs, K.M. Pos, Transport of drugs by the multidrug transporter AcrB involves an access and a deep binding pocket that are separated by a switch-loop, *Proc. Natl. Acad. Sci.* 109 (2012) 5687–5692.
- [17] F. Husain, H. Nikaido, Substrate path in the AcrB multidrug efflux pump of *Escherichia coli*, *Mol. Microbiol.* 78 (2010) 320–330.
- [18] F. Husain, M. Bikhchandani, H. Nikaido, Vestibules are part of the substrate path in the multidrug efflux transporter AcrB of *Escherichia coli*, *J. Bacteriol.* 193 (2011) 5847–5849.
- [19] R. Nakashima, K. Sakurai, S. Yamasaki, K. Nishino, A. Yamaguchi, Structures of the multidrug exporter AcrB reveal a proximal multisite drug-binding pocket, *Nature* 480 (2011) 565–569.
- [20] C. Oswald, H.-K. Tam, K.M. Pos, Transport of lipophilic carboxylates is mediated by transmembrane helix 2 in multidrug transporter AcrB, *Nat. Commun.* 7 (2016) 13819.
- [21] M. Zwama, S. Yamasaki, R. Nakashima, K. Sakurai, K. Nishino, A. Yamaguchi, Multiple entry pathways within the efflux transporter AcrB contribute to multidrug recognition, *Nat. Commun.* 9 (2018).
- [22] A.V. Vargiu, H. Nikaido, Multidrug binding properties of the AcrB efflux pump characterized by molecular dynamics simulations, *Proc. Natl. Acad. Sci.* 109 (2012) 20637–20642.
- [23] A. Ababou, V. Koronakis, Structures of gate loop variants of the AcrB drug efflux pump bound by erythromycin substrate, *PLoS One* 11 (2016) e0159154.
- [24] H.-j. Cha, R.T. Muller, K.M. Pos, Switch-loop flexibility affects transport of large drugs by the promiscuous AcrB multidrug efflux transporter, *Antimicrob. Agents Chemother.* 58 (2014) 4767–4772.
- [25] R.T. Müller, T. Travers, H. Cha, J.L. Phillips, S. Gnanakaran, K.M. Pos, Switch loop flexibility affects substrate transport of the AcrB efflux pump, *J. Mol. Biol.* 429 (2017) 3863–3874.
- [26] R. Nakashima, K. Sakurai, S. Yamasaki, K. Hayashi, C. Nagata, K. Hoshino, Y. Onodera, K. Nishino, A. Yamaguchi, Structural basis for the inhibition of bacterial multidrug exporters, *Nature* 500 (2013) 102–106.
- [27] H. Sjuts, A.V. Vargiu, S.M. Kwasny, S.T. Nguyen, H.-S. Kim, X. Ding, A.R. Ornik, P. Ruggerone, T.L. Bowlin, H. Nikaido, K.M. Pos, T.J. Opperman, Molecular basis for inhibition of AcrB multidrug efflux pump by novel and powerful pyranopyridine derivatives, *Proc. Natl. Acad. Sci.* 113 (2016) 3509–3514.
- [28] A.V. Vargiu, P. Ruggerone, T.J. Opperman, S.T. Nguyen, H. Nikaido, Molecular mechanism of MBX2319 inhibition of *Escherichia coli* AcrB multidrug efflux pump and comparison with other inhibitors, *Antimicrob. Agents Chemother.* 58 (2014) 6224–6234.
- [29] V.K. Ramaswamy, P. Cacciotto, G. Mallocci, A.V. Vargiu, P. Ruggerone, Computational modelling of efflux pumps and their inhibitors, *Essays Biochem.* 61 (2017) 141–156.
- [30] A.V. Vargiu, V.K. Ramaswamy, G. Mallocci, I. Malvacio, A. Atzori, P. Ruggerone, Computer simulations of the activity of RND efflux pumps, *Res. Microbiol.* 169 (2018) 384–392.
- [31] J.M.A. Blair, L.J.V. Piddock, How to measure export via bacterial multidrug resistance efflux pumps, *MBio* 7 (2016) (e00840-16).
- [32] V.K. Ramaswamy, A.V. Vargiu, G. Mallocci, J. Dreier, P. Ruggerone, Molecular rationale behind the differential substrate specificity of bacterial RND multi-drug transporters, *Sci. Rep.* 7 (2017).
- [33] Ombrato, R. Garofalo, B. Mangano, G. Capezzone de Joannon, A. Corso, G. Cavarischia, C. Furlotti, G. Iacoangeli, T. Antibacterial compounds having broad spectrum activity, patent number: WO2016096686A1.
- [34] CLSI, Methods for Dilution Antimicrobial Susceptibility testing of Anaerobic bacteria; Approved Standard-Eighth Edition M11-A8, Clinical and Laboratory Standards Institute, Wayne, PA, USA, 2012.
- [35] CLSI, Methods for Dilution Antimicrobial Susceptibility test for Bacteria That Grow Aerobically; Approved Standard-Tenth Edition M07-A10, Clinical and Laboratory Standards Institute, Wayne, PA, USA, 2015.
- [36] CLSI, Performance standards for antimicrobial susceptibility testing Twenty-Fifth Informational Supplement M100-S25, Clinical and Laboratory Standards Institute, Wayne, PA, USA, 2015.
- [37] R. Buonfiglio, M. Recanatini, M. Masetti, Protein flexibility in drug discovery: from theory to computation, *ChemMedChem* 10 (2015) 1141–1148.
- [38] S.-Y. Huang, X. Zou, Ensemble docking of multiple protein structures: considering protein structural variations in molecular docking, *Proteins* 66 (2007) 399–421.
- [39] W. Sinko, S. Lindert, J.A. McCammon, Accounting for receptor flexibility and enhanced sampling methods in computer aided drug design, *Chem. Biol. Drug Des.* 81 (2013).
- [40] R.A. Friesner, R.B. Murphy, M.P. Repasky, L.L. Frye, J.R. Greenwood, T.A. Halgren, P.C. Sanschagrin, D.T. Mainz, Extra precision glide: docking and scoring incorporating a model of hydrophobic enclosure for protein–ligand complexes, *J. Med. Chem.* 49 (2006) 6177–6196.
- [41] J.A. Maier, C. Martinez, K. Kasavajhala, L. Wickstrom, K.E. Hauser, C. Simmerling, ffl4SB: improving the accuracy of protein side chain and backbone parameters from ff99SB, *J. Chem. Theory Comput.* 11 (2015) 3696–3713.
- [42] J. Wang, R.M. Wolf, J.W. Caldwell, P.A. Kollman, D.A. Case, Development and testing of a general AMBER force field, *J. Comput. Chem.* 25 (2004) 1157–1174.
- [43] N. Tsukagoshi, R. Aono, Entry into and release of solvents by *Escherichia coli* in an organic-aqueous two-liquid-phase system and substrate specificity of the AcrAB-ToIC solvent-extruding pump, *J. Bacteriol.* 182 (2000) 4803–4810.
- [44] D.A. Case, D.S. Cerutti, T.E. Cheatham, T.A. Darden, R.E. Duke, T.J. Giese, H. Gohlke, A.W. Goetz, D. Greene, N. Homeyer, S. Izadi, A. Kovalenko, T.S. Lee, S. LeGrand, P. Li, C. Lin, J. Liu, T. Luchko, R. Luo, D. Mermelstein, et al., AMBER16, University of California, San Francisco, University of California, San Francisco, 2017.
- [45] D. Du, Z. Wang, N.R. James, J.E. Voss, E. Klimont, T. Ohene-Agyei, H. Venter, W. Chiu, B.F. Luisi, Structure of the AcrAB-ToIC multidrug efflux pump, *Nature* 509 (2014) 512–515.
- [46] H.M. Berman, The Protein Data Bank, *Nucleic Acids Res.* 28 (2000) 235–242.
- [47] Schrödinger LigPrep, LLC, New York, NY, (2015).
- [48] J.R. Greenwood, D. Calkins, A.P. Sullivan, J.C. Shelley, Towards the comprehensive, rapid, and accurate prediction of the favorable tautomeric states of drug-like molecules in aqueous solution, *J. Comput. Aided Mol. Des.* 24 (2010) 591–604.
- [49] J.C. Shelley, A. Cholleti, L.L. Frye, J.R. Greenwood, M.R. Timlin, M. Uchimaya, Epik: a software program for pK(a) prediction and protonation state generation for drug-like molecules, *J. Comput. Aided Mol. Des.* 21 (2007) 681–691.
- [50] K.S. Watts, P. Dalal, R.B. Murphy, W. Sherman, R.A. Friesner, J.C. Shelley, ConfGen: a conformational search method for efficient generation of bioactive conformers, *J. Chem. Inf. Model.* 50 (2010) 534–546.
- [51] R.A. Friesner, J.L. Banks, R.B. Murphy, T.A. Halgren, J.J. Klicic, D.T. Mainz, M.P. Repasky, E.H. Knoll, M. Shelley, J.K. Perry, D.E. Shaw, P. Francis, P.S. Shenkin, Glide: a new approach for rapid, accurate docking and scoring 1 method and assessment of docking accuracy, *J. Med. Chem.* 47 (2004) 1739–1749.
- [52] T.A. Halgren, R.B. Murphy, R.A. Friesner, H.S. Beard, L.L. Frye, W.T. Pollard, J.L. Banks, Glide: a new approach for rapid, accurate docking and scoring 2 enrichment factors in database screening, *J. Med. Chem.* 47 (2004) 1750–1759.
- [53] M.R. Berthold, N. Cebron, F. Dill, T.R. Gabriel, T. Kötter, T. Meinel, P. Ohl, C. Sieb, K. Thiel, B. Wiswedel, KNIME: The Konstanz information miner, *Data Anal. Mach. Learn. Appl.*, Springer, Berlin, Heidelberg, 2008, pp. 319–326.
- [54] L. Marsh, Strong ligand-protein interactions derived from diffuse ligand interactions with loose binding sites, *Biomed. Res. Int.* 2015 (2015) e746980.
- [55] A. Atzori, V.N. Malviya, G. Mallocci, J. Dreier, K.M. Pos, A.V. Vargiu, P. Ruggerone, Identification and characterization of carbapenem binding sites within the RND-transporter AcrB, *Biochim. Biophys. Acta Biomembr.* 1861 (2019) 62–74.
- [56] S. Genheden, U. Ryde, The MM/PBSA and MM/GBSA methods to estimate ligand-binding affinities, *Expert Opin. Drug Discovery* 10 (2015) 449–461.
- [57] C.J. Dickson, B.D. Madej, Á.A. Skjerveik, R.M. Betz, K. Teigen, I.R. Gould, R.C. Walker, Lipid14: the Amber lipid force field, *J. Chem. Theory Comput.* 10 (2014) 865–879.
- [58] W.L. Jorgensen, J. Chandrasekhar, J.D. Madura, R.W. Impey, M.L. Klein, Comparison of simple potential functions for simulating liquid water, *J. Chem. Phys.* 79 (1983) 926–935.
- [59] I.S. Jeong, T.E. Cheatham, Determination of alkali and halide monovalent ion parameters for use in explicitly solvated biomolecular simulations, *J. Phys. Chem. B* 112 (2008) 9020–9041.
- [60] M.J. Frisch, G.W. Trucks, H.B. Schlegel, G.E. Scuseria, M.A. Robb, J.R. Cheeseman, G. Scalmani, V. Barone, B. Mennucci, G.A. Petersson, H. Nakatsuji, M. Caricato, X. Li, H.P. Hratchian, A.F. Izmaylov, J. Bloino, G. Zheng, J.L. Sonnenberg, M. Hada, M. Ehara, et al., Gaussian 09, Revision B01, Gaussian, Inc., Wallingford CT, 2010.
- [61] G. Mallocci, A. Vargiu, G. Serra, A. Bosin, P. Ruggerone, M. Ceccarelli, A database of force-field parameters, dynamics, and properties of antimicrobial compounds, *Molecules* 20 (2015) 13997–14021.
- [62] C.W. Hopkins, S. Le Grand, R.C. Walker, A.E. Roitberg, Long-time-step molecular dynamics through hydrogen mass repartitioning, *J. Chem. Theory Comput.* 11 (2015) 1864–1874.
- [63] T. Williams, C. Kelley, *gnuplot* 50, (n.d.).
- [64] W. Humphrey, A. Dalke, K. Schulten, VMD: Visual Molecular Dynamics, *J. Mol. Graph.* 14 (1996) 33–38.
- [65] A.D. Kinana, A.V. Vargiu, H. Nikaido, Some ligands enhance the efflux of other ligands by the *Escherichia coli* multidrug pump AcrB, *Biochemistry* 52 (2013) 8342–8351.
- [66] A.D. Kinana, A.V. Vargiu, T. May, H. Nikaido, Aminoacyl β -naphthylamides as substrates and modulators of AcrB multidrug efflux pump, *Proc. Natl. Acad. Sci.* 113 (2016) 1405–1410.
- [67] H. Gohlke, C. Kiel, D.A. Case, Insights into protein-protein binding by binding free energy calculation and free energy decomposition for the Ras-Raf and Ras-RalGDS complexes, *J. Mol. Biol.* 330 (2003) 891–913.
- [68] Z. Feng, T. Hou, Y. Li, Unidirectional peristaltic movement in multisite drug binding pockets of AcrB from molecular dynamics simulations, *Mol. Biosyst.* 8 (2012) 2699.
- [69] B. Wang, J. Weng, W. Wang, Substrate binding accelerates the conformational transitions and substrate dissociation in multidrug efflux transporter AcrB, *Front. Microbiol.* 6 (2015).
- [70] E. Padilla, E. Llobet, A. Doménech-Sánchez, L. Martínez-Martínez, J.A. Bengoechea, S. Albertí, Klebsiella pneumoniae AcrAB efflux pump contributes to antimicrobial resistance and virulence, *Antimicrob. Agents Chemother.* 54 (2010) 177–183.
- [71] L. Sánchez, W. Pan, M. Viñas, H. Nikaido, The acrAB homolog of *Haemophilus influenzae* codes for a functional multidrug efflux pump, *J. Bacteriol.* 179 (1997) 6855–6857.
- [72] C. Wandersman, P. Delepelaire, TolC, an *Escherichia coli* outer membrane protein required for hemolysin secretion, *Proc. Natl. Acad. Sci.* 87 (1990) 4776–4780.
- [73] T. Imai, N. Miyashita, Y. Sugita, A. Kovalenko, F. Hirata, A. Kidera, Functionality mapping on internal surfaces of multidrug transporter AcrB based on molecular theory of solvation: implications for drug efflux pathway, *J. Phys. Chem. B* 115 (2011) 8288–8295.
- [74] A.R. Leach, B.K. Shoichet, C.E. Peishoff, Prediction of protein–ligand interactions

- docking and scoring: successes and gaps, *J. Med. Chem.* 49 (2006) 5851–5855.
- [75] G.L. Warren, C.W. Andrews, A.-M. Capelli, B. Clarke, J. LaLonde, M.H. Lambert, M. Lindvall, N. Nevins, S.F. Semus, S. Senger, G. Tedesco, I.D. Wall, J.M. Woolven, C.E. Peishoff, M.S. Head, A critical assessment of docking programs and scoring functions, *J. Med. Chem.* 49 (2006) 5912–5931.
- [76] A.A. Neyfakh, Mystery of multidrug transporters: the answer can be simple, *Mol. Microbiol.* 44 (2002) 1123–1130.
- [77] A.D. Kinana, A.V. Vargiu, H. Nikaïdo, Effect of site-directed mutations in multidrug efflux pump AcrB examined by quantitative efflux assays, *Biochem. Biophys. Res. Commun.* 480 (2016) 552–557.
- [78] A.V. Vargiu, F. Collu, R. Schulz, K.M. Pos, M. Zacharias, U. Kleinekathöfer, P. Ruggerone, Effect of the F610A mutation on substrate extrusion in the AcrB transporter: explanation and rationale by molecular dynamics simulations, *J. Am. Chem. Soc.* 133 (2011) 10704–10707.
- [79] A.V. Vargiu, V.K. Ramaswamy, I. Malvacio, G. Malloci, U. Kleinekathöfer, P. Ruggerone, Water-mediated interactions enable smooth substrate transport in a bacterial efflux pump, *Biochim. Biophys. Acta Gen. Subj.* 1862 (2018) 836–845.
- [80] R. Patil, S. Das, A. Stanley, L. Yadav, A. Sudhakar, A.K. Varma, Optimized hydrophobic interactions and hydrogen bonding at the target-ligand interface leads the pathways of drug-designing, *PLoS One* 5 (2010) e12029.
- [81] H.-J. Böhm, D. Banner, S. Bendels, M. Kansy, B. Kuhn, K. Müller, U. Obst-Sander, M. Stahl, Fluorine in medicinal chemistry, *ChemBioChem* 5 (2004) 637–643.
- [82] S.G. DiMaggio, H. Sun, The strength of weak interactions: aromatic fluorine in drug design, *Curr. Top. Med. Chem.* 6 (2006) 1473–1482.
- [83] V.K. Ramaswamy, A.V. Vargiu, G. Malloci, J. Dreier, P. Ruggerone, Molecular determinants of the promiscuity of MexB and MexY multidrug transporters of *Pseudomonas aeruginosa*, *Front. Microbiol.* 9 (2018).